1966), p. 293.
[24]O. S. Oen, D. K. Holmes, and M. T. Robinson, U. S. Atomic Energy Commission Report No. ORNL-3017, 1960 (unpublished).
[25]H. Rosenstock, second following paper, Phys. Rev. B 5, 1402 (1972).

PHYSICAL REVIEW B VOLUME 5, NUMBER 4 15 FEBRUARY 1972

Contribution of Defect Dragging to Dislocation Damping. II. Experimental*

H. M. Simpson,† A. Sosin, and D. F. Johnson‡
Department of Physics, University of Utah, Salt Lake City, Utah 84112
(Received 26 August 1971)

Detailed internal-friction and Young's-modulus measurements have been made in electron-irradiated copper. The measurements confirm the defect-dragging-model calculations presented in the previous paper. In particular, an initial increase and subsequent decrease in logarithmic decrement δ is observed. This peaking effect is shown to be highly structurally dependent, vanishing after a suitable high-temperature annealing treatment. The proportionality of δ to the modulus defect $\Delta E/E$ is demonstrated. This dependence, contrary to previous expectations that $\delta \propto (\Delta E/E)^2$, is consistent with the dragging model. Agreement with the dragging model is quite complete if two types of dislocations are assumed, as has been reported by other investigators.

I. INTRODUCTION

In the previous paper,[1] we have developed a model for dislocation damping in metals—actually a low-frequency extension of the Koehler-Granato-Lücke (KGL) model.[2,3] The predictions of this new formulation explain some of the discrepancies noted by many observers but rarely documented in any sufficient detail. Furthermore, the formulation's predictions are notably different from those predictions investigators have generally drawn—incorrectly—from the KGL theory.

This paper presents a more detailed investigation of damping at relatively low frequencies, to test the predictions of our newer model.

II. EXPERIMENTAL PROCEDURE

A. Sample Preparation

The experiments for this work were performed on high-purity (99.999%) copper from the American Smelting and Refining Company. The copper was received in an extruded and swaged rod $\frac{3}{8}$ in. in diameter. From this material a sample was machined into the shape of a cantilevered beam with active sample dimension in the form of a foil of thickness (about 0.006–0.007 in.), 1-cm length, and $\frac{1}{2}$-cm width. After machining, the sample was etched to a final thickness of 0.004–0.005 in. Copper samples of these dimensions usually have a natural resonant frequency of about 500 Hz when resonated in the flexural mode. Following the final etch, samples were mounted in the appropriate irradiation apparatus without any intervening heat treatment. The samples were polycrystalline.

B. Equipment

Our experimental arrangement allows us to continuously (every 2–3 sec) monitor the logarithmic decrement and Young's modulus as a function of time. To do this we employ a capacitive pickup system (the sample forms half of a parallel-plate capacitor) similar to that described by DiCarlo *et al.*,[4] but with the advantage of automatic data logging.

It can be shown[5] that the decrement can be related to the force F required to maintain a damped harmonic oscillator vibrating at constant amplitude through

$$\delta = \delta_0(\omega/\omega_0)^2 F/F_0 , \tag{1}$$

where the subscript 0 refers to preirradiation values. Young's modulus E is obtained from the resonant frequency of the bar by

$$E = kf^2 . \tag{2}$$

The force acting on the sample is proportional to the square of the voltage impressed across the sample and drive plate. This voltage will be referred to as the drive voltage. The decrement is now given by

$$\delta = \delta_0(\omega/\omega_0)^2 V^2/V_0^2 . \tag{3}$$

Usually $\omega/\omega_0 \sim 1$, and so $\delta \propto V^2$. To measure δ_0, the signal from the freely decaying sample amplitude is stored in a storage scope. A photograph is taken and the log decrement measured in the usual manner. It is difficult to estimate uncertainty limits u in the relative changes in the decrement and Young's modulus, but typical values would be

$u(\delta) \sim 3 \times 10^{-2}$ and $u(E) \sim 10^{-5}$, respectively. This latter number depends on both the temperature stability $[(1/E)\, dE/dT \sim 0.1\%/^{\circ}\mathrm{K}]$ and the actual log decrement; the lower the value of δ, the more accurately the frequency can be measured. To increase the accuracy in the modulus readings, the period is usually averaged over 10^3 periods.

The flow diagram for the equipment which is used to monitor the decrement (drive voltage) and Young's modulus (period) is presented in Fig. 1. The sample forms one plate of a parallel-plate capacitor which is in the tank circuit of a high-frequency oscillator. Thus, motion of the sample is translated into a frequency deviation of the fm oscillator. A frequency-deviation meter converts this motion into a signal which is proportional to the amplitude of the sample. The output from the deviation meter is fed through a variable-bandpass filter into a tuned amplifier—through a manual phase adjuster—buffer amplifier and into a voltage regulator and frequency divider ($\frac{1}{2}f$) with an output in the form of a square wave. This output is fed into a tuned amplifier where it is converted to a sine wave and then fed into the amplitude controller. This device compares the signal from the deviation meter with a reference signal and develops an error signal which controls the output of the tuned amplifier. Finally, the signal from the tuned amplifier is amplified by the driver amplifier, goes through an rf filter and is impressed across the sample and drive plate. An example of the raw data for the period is given in Fig. 2. This data was recorded digitally and then plotted on a Gerber plotter. The abrupt changes in the period and drive voltage result from the manual adjustment of the phase.

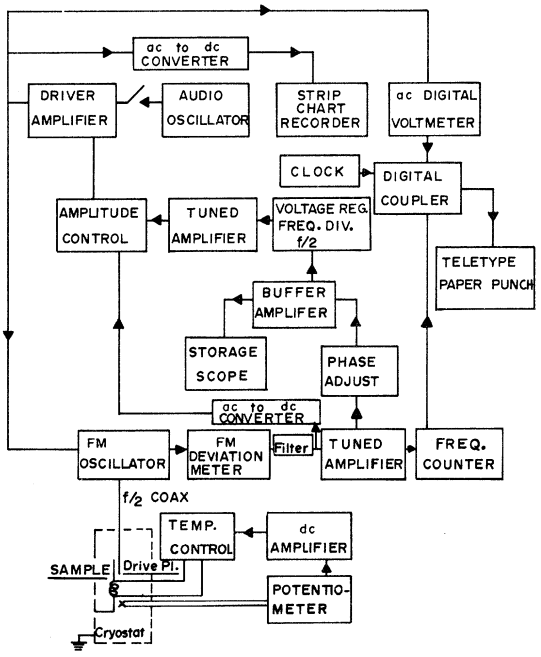

FIG. 1. Flow chart of the electronics which automatically records the logarithmic decrement and Young's modulus.

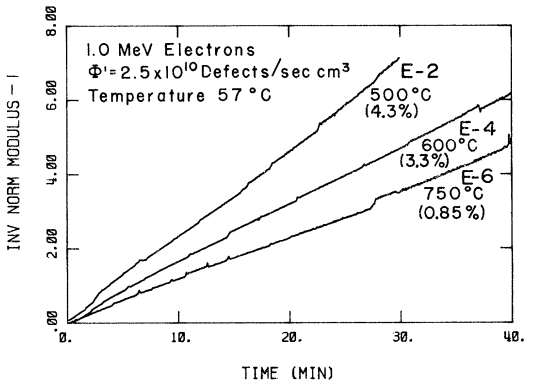

FIG. 2. Inverse normalized modulus defect minus one plotted as a function of irradiation time. Numbers beside each curve give the annealing temperature and the modulus defect prior to irradiation.

The strain amplitude used in any particular experiment is limited mainly by microphonic pickup, spurious vibrations transmitted from the accelerator, and the boiling of cryogenic liquids. Typically, a lower limit for the strain amplitude during a radiation-damage experiment is in the range 10^{-6}–10^{-7}. However, the electronic apparatus is capable of easily measuring a strain amplitude as low as 10^{-8}. Amplitude dependence was almost completely absent.

In a typical operating procedure, a sample is annealed at 500 °C for 10 min. This treatment restores the sample to its preirradiation state. The sample then is lowered to the desired temperature and irradiation proceeds.

In interpreting the data, it is necessary to establish "elastic" or "saturation" values of the decrement δ_e and Young's modulus E_e. The treatment which has been shown[6] to this purpose—the one we have used—is to raise the sample temperature to 100 °C and hold there for 10 min. This thermal procedure, following even the small electron fluences used in much of our work, is sufficient to guarantee that the radiation-produced point defects arrive at dislocations in sufficient number to eliminate essentially all dislocation contribution to internal-friction and elastic-moduli values.

Irradiation experiments are performed with a sample housed in one of three chambers, each of which can operate at any temperature from a lower temperature (4, 78, and 300 °K, respectively) to 1050 °K. The uncertainty in the sample temperature during any particular irradiation is, at most, 0.02 °K below 300 °K. All temperature measure-

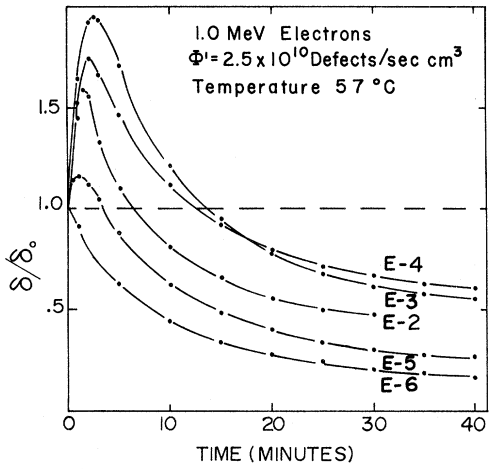

FIG. 3. Decrement normalized to its preirradiation value and plotted as a function of irradiation time. See Table I for data related to each run.

ments were made with an iron-constantan thermocouple.

III. EXPERIMENTAL RESULTS

We have previously reported[7,8] preliminary results on the effects of electron irradiation on the decrement and Young's modulus in copper. These data showed that under certain conditions the decrement *increased* due to irradiation, contrary to the usually observed behavior. To investigate this "peaking effect" further, we have performed an extended series of irradiations on one pure copper sample. Each irradiation with 1-MeV electrons was performed on this sample and the temperature of irradiation (57 °C) was constant for each run. Also a constant electron flux of 5.7×10^{10} electrons/cm^2 sec (for about 40 min) leading to a Frenkel pair-production rate (excluding close pair recombination) of about 2.5×10^{10} defects/cm^3 sec was maintained. The primary purpose of this set of experiments was to determine the influence of the thermal annealing treatment on the decrement and on the modulus defect, as a function of irradiation dose.

The results for the decrement are presented in Fig. 3 and Table I. One run ($E-1$) was performed on the as-mounted sample (with no previous annealing treatment) with the result that neither the decrement nor modulus changed appreciably after irradiation with $\sim 3\times10^{14}$ electrons/cm^2. The pertinent data for each run are presented in Table I. Note that annealing the sample at 500 °C for 30 min gave, upon the next irradiation, a maximum decrement δ_p equal to about 1.6 times the initial decrement δ_0. Reannealing at 500 °C for 10 min and then performing identical irradiation ($E-3$) gave a peak height of 1.95. Raising the annealing temperature caused the peak height to diminish until at 750 °C ($E-6$) the "peaking effect" is completely eliminated. Subsequently, annealing at 500 °C and performing the standard irradiation did not give the peaking effect (see Fig. 4).

Apparently, for samples with our history, the critical annealing temperature range for eliminating the peaking effect is near 750 °C. Also note from Fig. 3, that as the peak height is reduced the peak position shifts toward zero time. From Table I we see roughly that as the peak height is reduced the preirradiation value of the decrement δ_0 increases.

The previously discussed peaking effect has been observed by us in a number of samples, all with the same thermal history. Thus, its validity is well established. Indeed it appears to be even more universal, since we have recently observed a peaking effect in the decrement in high-purity aluminum resonated at about 1 KHz. In addition, a peaking effect was observed by Nielsen[9] during proton bombardment of copper at 20 °K, but Nielsen largely disregarded this effect. We were unaware of Nielsen's results during the course of the work. Note particularly the large temperature difference between the work of Nielsen and our present work.

Simultaneously with the decrement measurements we also measured the changes in Young's modulus, and these results are given in Fig. 2 and Table I.

TABLE I. Important data for runs $E-2$ through $E-8$.

Run	Annealing Temp (°C)	Annealing Time (min)	δ_0	δ_e	δ_{peak}/δ_0	$\left(\frac{\Delta E}{E}\right)_0$	$\frac{d}{dt}\left(\frac{\Delta E}{E}\right)_0 \Big/ \left(\frac{\Delta E}{E}\right)$ (min^{-1})
$E-2$	500	30	0.00352	0.00103	1.596	0.043	0.229
$E-3$	500	10	0.00359	0.00116	1.948	0.047	0.192
$E-4$	600	30	0.00260	0.00074	1.745	0.033	0.153
$E-5$	700	30	0.00351	0.00049	1.164	0.021	0.165
$E-6$	750	30	0.00446	0.00036	No peak	0.014	0.150
$E-7$	500	10	0.00406	0.00033	No peak	0.0088	0.101
$E-8$	750	30	0.00330	0.00033	No peak	0.0085	0.119

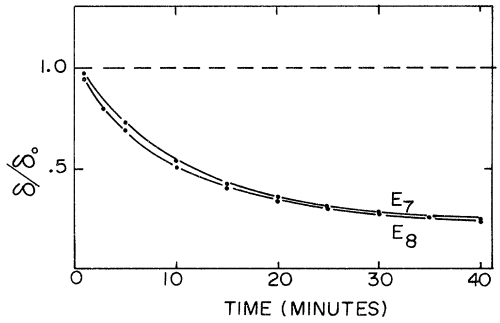

FIG. 4. Decrement normalized to its preirradiation value and plotted as a function of irradiation time. See Table I for data related to each run.

The quantity plotted along the ordinate is the inverse normalized modulus defect minus one, which is defined as

$$\varphi^{-1} \equiv [(\Delta E/E_0)/(\Delta E/E)] - 1 \,. \tag{4}$$

These plots are taken from the raw data as they are plotted out point by point by a Gerber plotter. The striking feature of the data is the apparent linearity of φ^{-1} as a function of time. Note from Table I that both the total modulus defect and its time-rate of change vary considerably depending on the annealing treatment. In particular, from run $E-2$ (500 °C anneal) to $E-8$ (750 °C anneal) the modulus defect changes by a factor of more than five. Nevertheless, the linearity of the modulus data with time is preserved. This is an indication that the same basic processes are operative for all the experiments. This same conclusion should also apply to the decrement data.

Additional data were obtained on another sample which had been annealed at 750 °C for $\frac{1}{2}$ h. These results are presented in Fig. 5. The normalized inverse decrement $\Delta\delta_0/\Delta\delta$ is defined as follows:

$$\frac{\Delta\delta_0}{\Delta\delta} \equiv \frac{\delta_0 - \delta_e}{\delta - \delta_e} \,. \tag{5}$$

The subscript e refers to the elastic values, i.e., the values after all dislocation motion is fully restricted. The production rate for this data was 5.57×10^{10} electrons/cm^2 sec. Again, note the linearity of these data with time after a short initial time interval.

A series of experiments was also performed on a third sample. Here the primary interest was in the temperature dependence of the pinning rate. Irradiations were performed over the temperature range 290–410 °K. The sample had previously been annealed at 750 °C for $\frac{1}{2}$ h; a peak did not occur in the decrement-vs-time plot. Results for this set of experiments are given in Figs. 6 and 7. These data extend to larger changes in the decrement and

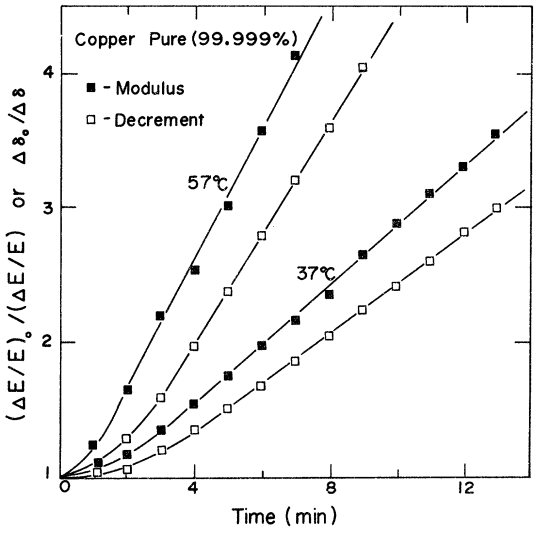

FIG. 5. Normalized inverse modulus defect and decrement plotted as a function of irradiation time for the indicated temperatures.

modulus and the results show that, for higher defect densities, φ^{-1} and $\Delta\delta_0/\Delta\delta$ are no longer linear in time. A more rapid increase in these quantities with time is evident.

Additional information can be gleaned from the data presented in Figs. 5–7, by plotting the normalized decrement vs the normalized modulus defect. Such plots are given in Figs. 8 and 9. These data show that the modulus and decrement have about the same dependence on the density of point

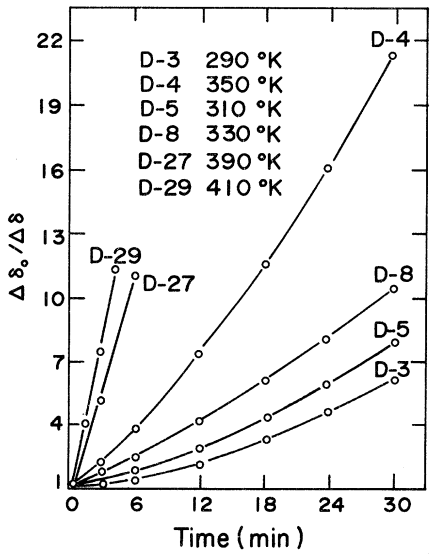

FIG. 6. Inverse normalized decrement plotted as functions of irradiation time for the indicated temperatures.

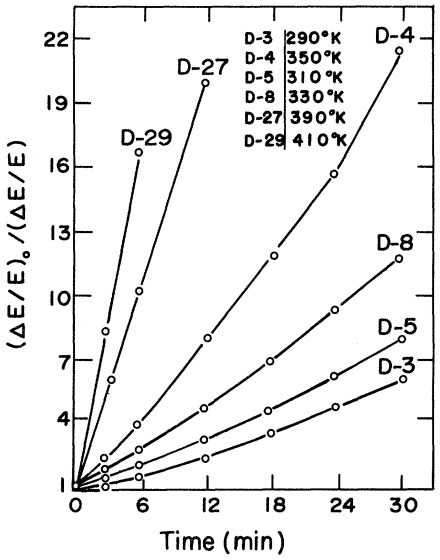

FIG. 7. Inverse normalized modulus defect plotted as a function of irradiation time for the indicated temperature.

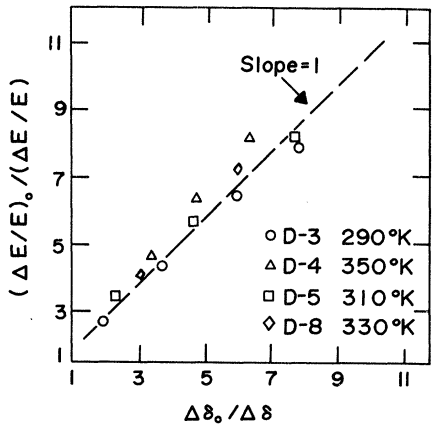

FIG. 9. Inverse normalized modulus defect vs the inverse normalized decrement for the data from Figs. 6 and 7.

defects on dislocations. The highly important significance of this plot lies in the fact that time and/or diffusion kinetics do not play any significant role, since both modulus and decrement values are determined by the same number of point defects on dislocations. These plots demonstrate convincingly that, for our experimental conditions, the frequently cited l^2-l^4 dependences in modulus defect and decrement, respectively, are not valid (l is generally taken as the length of dislocation segments between pinning points; see the previous paper).

IV. DISCUSSION

The experimental results presented in Sec. III clearly show that the usual interpretation of pinning experiments in terms of the KGL theory is not valid for our work. This is evidenced most dramatically by the qualitative features of the peaking effect in the decrement and also by the simple proportionality between the modulus and decrement. Both of these observations are at odds with the KGL theory as it is usually interpreted in terms of point defects acting as firm pinning points. From the calculations of paper I, we see that a number of the qualitative features of the data can be described by the dragging model, most notably the peaking effect.

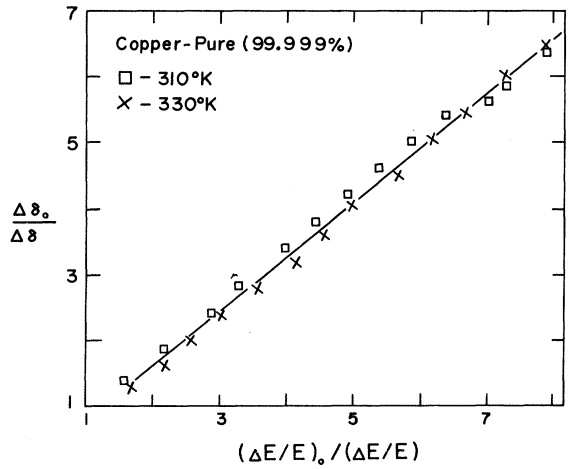

FIG. 8. Inverse normalized decrement vs the inverse normalized modulus defect for the data of Fig. 5.

Detailed observations concerning the interaction of radiation-induced point defects with dislocations are complicated due to the following considerations: (i) In dynamic irradiation experiments at elevated temperatures, interstitials and vacancies are created in the lattice and then diffuse to dislocations. (ii) Point defects on dislocations can diffuse along the dislocation line and possibly form clusters or effectively disappear at nodal point traps. (iii) Possibly both interstitial and vacancies are diffusing to dislocations, each with its own diffusion constant. The above-mentioned complications make it difficult to calculate the number of point defects on dislocation lines from first principles. However, we should be able to arrive at the time law which describes the rate of arrival of defects at dislocations.

A plausible model which can account for the time dependence of the accumulation of point defects on dislocations is as follows: (i) Interstitials and vacancies are created in the lattice at a constant production rate φ' (this number excludes the fraction of interstitials and vacancies which recombine via close-pair and correlated recovery). The interstitial diffuses (characterized by a diffusion coefficient D) at a much greater rate than the vacancy.

The concentration of interstitials and vacancies are always small so interstitial-vacancy, interstitial-interstitial, etc., reactions can be ignored. Furthermore, at the temperatures of interest here (i.e., above 300 °K), impurities probably do not trap interstitials. (ii) Interstitials which are on dislocations can diffuse along the dislocation line with a diffusion coefficient D_L to nodal point traps. Clustering is ignored since resistivity studies show dimers to be unstable at these temperatures. Under these conditions we can write the following set of rate equations:

$$\frac{dc_i}{dt} = \varphi' - c_i D\Lambda \,, \tag{6}$$

$$\frac{dn_d}{dt} = c_i D l_0 - n_d K_N \,, \tag{7}$$

where c_i is the concentration of interstitials in the lattice, n_d is the number of interstitials trapped at dislocations, on an average length l_0 of dislocation line between nodes, Λ is the planar density of dislocations, and K_N is the rate at which interstitials leave the dislocation line at nodal points, regarded as deep traps for interstitials, along dislocations. It can be shown by considering the one-dimensional diffusional problem that (see Appendix A)

$$K_N = \pi^2 D_L / l_0^2 \,. \tag{8}$$

For production rates and times of interest here, $\varphi' \gg D c_i \Lambda$. Thus, Eq. (6) implies

$$c_i \simeq \varphi' t \,, \tag{9}$$

so that

$$n_d = (l_0 D \varphi' / K_N)[t - (1/K_N)(1 - e^{-K_N t})] \,. \tag{10}$$

After an initial transient, we see that

$$\frac{dn_d}{dt} = l_0 \varphi' \frac{D}{K_N} \,, \tag{11}$$

which gives a constant rate of accumulation of point defects on the dislocation lines. Equation (7) evaluated near $t = 0$ (i.e., with $c_i \simeq 0$, $n_d \simeq 0$) predicts that $dn_d/dt = 0$ initially. Thus this analysis predicts the functional behavior observed in Fig. 5—zero initial slope tending to a subsequent linear growth. It is important to note that the last term in Eq. (7), a loss term for the interstitial population on dislocations, is important. In the absence of this term, Eq. (7) predicts a parabolic growth pattern.

The matching of data, such as in Figs. 5–7 with the analysis in Eqs. (6)–(11) implies that

$$n_d \propto [(\Delta E/E)_0/(\Delta E/E) - 1] \tag{12}$$

and, in the absence of the peaking effect,

$$n_d \propto (\Delta\delta_0/\Delta\delta - 1) \,. \tag{13}$$

We take this to imply that

$$\frac{\Delta E}{E} = \left(\frac{\Delta E}{E}\right)_0 (1 + n_d)^{-1} = \left(\frac{\Delta E}{E}\right)_0 (1 + \alpha t)^{-1} \,, \tag{14}$$

except at early times (and at long times). In contrast, previous analysis was based on a $(1 + n_d)^{-2}$ dependence, rather than $(1 + n_d)^{-1}$. For the decrement, in the absence of the peaking effect, the usual $(1 + n_d)^{-4}$ dependence gives way here to a $(1 + n_d)^{-1}$ dependence also. The latter case particularly is a profound change in dependence on n_d.

Equation (11) also predicts, for experiments performed at different temperatures, that a plot of $\ln(dn_D/dt)$ vs T^{-1} should have a slope of $(E_m - E_L)/k$ and intercept of $\varphi' D_0 l_0^3/\pi^2 D_{L_0}$, where

$$D = D_0 e^{-E_m/kT}$$

and

$$D_L = D_{L_0} e^{-E_L/kT} \,.$$

To check the above analysis, a plot of pinning rates dn_d/dt for various temperatures is given in Fig. 10 for impure copper—data from Fig. 1 of Ref. 7. A value of 0.17 eV was obtained for $E_m - E_L$. This value compares favorably with the results of Thompson *et al.* in gamma-irradiated copper, who obtained $E_m - E_L \sim 0.2$ eV. In addition, we have performed a similar analysis for pulse-irradiation experiments and we obtained the same value for $E_m - E_L$. Thus, we have reasonable confidence that point defects are accumulating on the dislocations linearly with time during the time span of experiments such as ours. By evaluating the intercept in Fig. 12, we can calculate l_0 knowing that $\varphi' \approx 2.5 \times 10^{10}$ defects cm^{-3}sec^{-1}. The result is $l_0 \sim 7 \times 10^{-4}$ cm. This figure is characteristic of the values usually deduced in other internal-friction investigations, and once again emphasizes

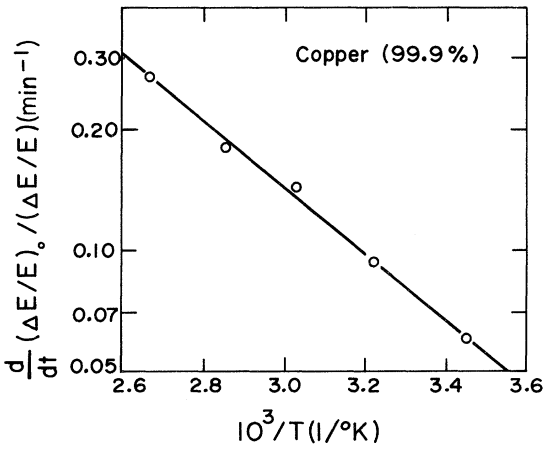

FIG. 10. Logarithm of the time rate of change of the normalized inverse modulus defect vs inverse temperature. Data were taken from Fig. 1 of Ref. 7.

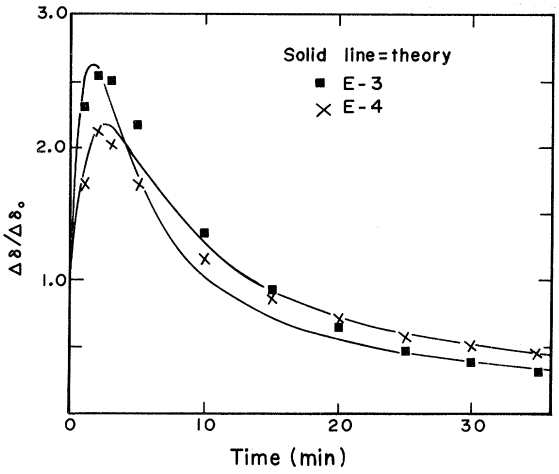

FIG. 11. Normalized decrement plotted as a function of irradiation time and compared with theory.

the long lengths which are implied, since $l_0 \gtrsim 10^4$ atoms distances.

An analysis of the peaking effect can now be performed by assuming that the number of dragging points increase linearly with time. Assuming that the dragging coefficient B for a dislocation increases linearly with the number of dragging points (interstitials), we have

$$B = B_0 + \gamma_B t \ . \tag{15}$$

We can now attempt to match the theoretical curve given in Fig. 1 of Ref. 1, to the experimental data of Fig. 3. To do this, we have used two fitting points: the peak height, and the fit at some arbitrary time. The theoretical curve was arbitrarily fitted to the data at time, $t = 30$ min (i. e., at relatively long times where the analysis should be most applicable). The results of this analysis are presented in Figs. 11 and 12. The parameters determined from this fit are listed in Table II. The fit is made using the parameter μ defined in the previous paper as

$$\mu^2 = (\omega l^2/2C)B \ , \tag{16}$$

so that

$$\mu^2 = \mu_0^2 + \gamma t \ , \tag{17}$$

with

$$\mu_0^2 = (\omega l^2/2C)B_0 \tag{18}$$

and

$$\gamma = (\omega l^2/2C)\gamma_B \ . \tag{19}$$

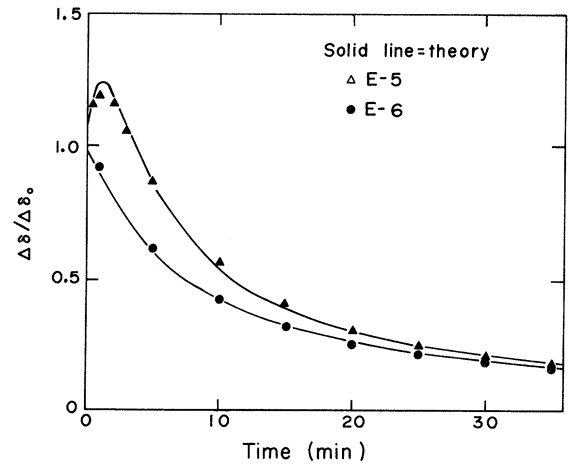

FIG. 12. Normalized decrement plotted as a function of irradiation time and compared with theory.

TABLE II. Parameters for theory fit.

Run No.	μ_0^2	γ
$E-3$	1.1	2.415
$E-4$	1.3	1.445
$E-5$	2.5	2.000
$E-6$	10.0	2.008

Note that for this analysis we have assumed that only B varies during the experiment. Although minor deviations do occur between theory and experiment, sufficient agreement exists to warrant belief in the basic tenets of the dragging model. This is particularly true when one considers that we have "smeared out" the defects along the dislocation line.

The previous treatment in terms of a single-dislocation type and a continuous distribution of defects along the dislocation line adequately accounts for the detailed time-dependent behavior of the decrement, however, so simple a picture is inadequate to account for the modulus data since it would predict that, at long times,

$$\Delta E/E \propto (1 + \alpha t)^{-3/2} \ , \tag{20}$$

a dependence which is not generally observed in detail. That is, at long times the modulus defect is observed to vary faster than linearly but fails to reach the $\frac{3}{2}$ power usually. As is true of so much in these experiments, the closeness in the approach to a $\frac{3}{2}$-power dependence depends on the history of the sample.

To explain the deviations from the long-time $\frac{3}{2}$-power prediction, and to account for the nonlinearities observed in Figs. 8 and 9, we would be forced to include the following complicating considerations to our simple models: (i) At long times, the kinetics culminating in Eq. (10), predict deviation from linear defect accumulation. The predicted deviation is toward a slower defect accumulation. (ii) At long times, interaction of defects, probably

leading to clustering, may occur along dislocations as the number of defects rises. Such interactions should also lead to slower apparent defect accumulations. (iii) Previous investigations, at higher frequencies, have indicated the existence of two distinct types of dislocations which contribute to dislocation damping. To examine the effect of this complication, we shall assume *ad hoc* (a) that point defects do firmly pin one of these dislocations types (type I, say)—i. e., the drag coefficient approaches infinity for this type of dislocation; and (b) the analysis for finite drag holds for type-II dislocations. The effect of pinning on type-I dislocations would then follow the "standard" dependence on pinning-point density n_{I} but the $\frac{3}{2}$-power dependence would prevail, at large fluences, for n_{II}. Considering the speculative nature of these assumptions, we have let $n_{\mathrm{I}} = n_{\mathrm{II}}$ and used equal lengths and dislocation densities to obtain the approximate expression for the modulus defect:

$$\frac{\Delta E}{E} \simeq \frac{\Lambda E b^2 l^2}{12C}\left(\frac{1}{(1+n)^2} + \frac{\beta}{(B_0/B_d+n)^{3/2}}\right), \quad (21)$$

with

$$\beta \equiv 2(12)^{1/2}(\omega B_d l/C)^{3/2} .$$

At this point, we may examine the inverse modulus defect $(\Delta E/E)^{-1}$ to see if it can increase linearly with with n. Taking the inverse of Eq. (21) we obtain

$$\left(\frac{\Delta E}{E}\right)^{-1} = \frac{12C}{\Lambda E b^2 l^2}\left(\frac{(1+n)^2}{1+\beta(1+n)^2(B_0/B_d+n)^{-3/2}}\right). \quad (22)$$

Although (22) is not analytically linear in n, it may be possible for it to approximate closely a limited linearity in n over a restricted range. That this is indeed true is shown by the plot of $(\Delta E/E)^{-1}$ $\Lambda E b^2 l^2/12C$ vs n in Fig. 13 for values of $B_0/B_d = 7$ and $\beta = 5.75$. Note the excellent linearity over at least an order-of-magnitude variation in $(\Delta E/E)^{-1}$. Attaching further physical significance to the values of B_0/B_d and β is, we feel, premature and somewhat hazardous. Mainly this analysis does show that it is possible for the inverse modulus defect to increase linearly with the addition of dragging points. Note that the corresponding consideration of decrement would call for the inclusion of a term proportional to $(1+n)^{-4}$ which would be small (see paper I) and rapidly decreasing. Accordingly, the decrement should be dominated by the type-II dislocations and the resulting energy losses associated with dragged point defects.

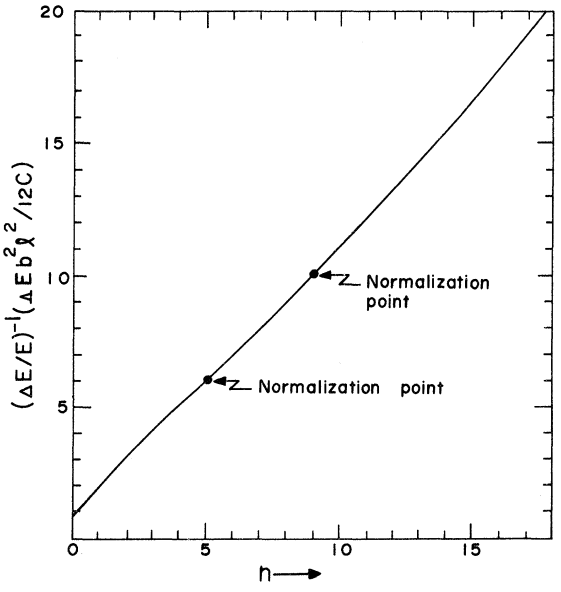

FIG. 13. Inverse normalized modulus defect for the two dislocation component model plotted as a function of n, the number of defects per dislocation segment.

A similar analysis could be performed with the adoption of two dislocation components, each dragging point defects. While a fit to the modulus data could probably be obtained using two $\frac{3}{2}$-power terms, fitting the decrement would be more difficult since each term here should be first power and, therefore, contribute substantially throughout the entire observations.

V. CONCLUSIONS

The data presented in this paper demonstrate that the usual (but incorrect) interpretation of radiation-damage experiments based on the firm-pinning-point KGL model is not valid in copper at relatively low frequencies. The presence of an initial increase and subsequent peak in the decrement upon irradiation is completely at variance with this "standard" pinning analysis. The direct proportionality of the decrement and the modulus defect during bombardment is also at variance with the renowned dependence: $\delta \propto (AE/E)^2$.

All of the observations can be accounted for by our defect-dragging model in a qualitative manner at the very least. Surprisingly good quantitative agreement is obtained with the single additional assumption of two dislocation species, one with a finite B and one with an infinite B. The essential features of the data can be fully explained. In particular, the simple proportionality of the decrement to the modulus and the proportionality of the inverse normalized modulus defect and decrement with respect to time, and finally a reasonable model for the defect diffusion emerges when one applies the above concepts. Most notably, usual values of activation energies are obtained from this analysis. Although considerable room exists for improving our calculations—for example, the temperature dependence of the drag coefficient, distribution of dislocation length, orientation factors, etc., we feel that the important ingredients in the theory

of dislocation damping in metals are in hand with the inclusion of defect dragging.

ACKNOWLEDGMENT

We are pleased to acknowledge the valuable and enthusiastic assistance in these experiments of W. Even.

APPENDIX

To calculate the number of interstitials on a dislocation line, we consider the one-dimensional diffusion equation

$$\frac{\partial n(x,t)}{\partial t} = D_L \frac{\partial^2 n(x,t)}{\partial x^2} \tag{A1}$$

with boundary conditions

$$n(0,t) = n(l,t) = 0. \tag{A2}$$

The Green's function for this problem is[10]

$$G(x,x';t,t') = \frac{2}{l} \sum_{n=1}^{\infty} \exp\left(-\frac{D_L n^2 \pi^2 (t-t')}{l^2}\right) \times \sin\frac{n\pi x}{l} \sin\frac{n\pi x'}{l} . \tag{A3}$$

Equation (A3) gives the probability that if a particle starts out at the point x' at time t' then it will be at the point x at a later time t. Thus, we need to calculate a source function $S(x', t')$ which gives the number of particles that arrive from the lattice to the point x' during a time t'. According to Damask and Dienes,[11] the rate of depletion of interstitials from the lattice due to dislocations is

$$\frac{dc_i}{dt} = -\Lambda D c_i . \tag{A4}$$

For us $c_i \simeq \varphi' t$; thus, the source function is

$$S(x', t') = D\varphi' t' . \tag{A5}$$

Now

$$n(x,t) = \int_0^l \int_0^t G(x,x';t,t') S(x',t')\, dx'\, dt' \tag{A6}$$

or

$$n(x,t) = \frac{4D\varphi'}{\pi l} \sum_{n=1 \text{odd} n}^{\infty} \int_0^t dt' \times \frac{t'}{n} \exp\left(-\frac{D_L n^2 \pi^2 (t-t')}{l^2}\right) \sin\frac{n\pi x}{l} . \tag{A7}$$

We are interested in $n_d(t)$, the number of defects present on a dislocation segment which is just the average of $n(x, t)$ over x,

$$n_d(t) = \frac{8D\varphi'}{\pi^2} \sum_{n=1 \text{odd} n}^{\infty} \int_0^t dt' \times \frac{t'}{n^2} \exp\left(-\frac{D_L n^2 \pi^2 (t-t')}{l^2}\right) . \tag{A8}$$

Since the terms in this series diminish rapidly, we need only the $n = 1$ term. With the identification of

$$K_N = D_L \pi^2 / l^2 \tag{A9}$$

we obtain

$$n_d(t) = \frac{8}{\pi^2} \frac{lD\varphi'}{K_N} \left(t - \frac{1}{K_N}(1 - e^{-K_N t})\right) . \tag{A10}$$

This expression differs from Eq. (5) only in the amount that $8/\pi^2$ deviates from unity.

---

*Research supported by the Metallurgy and Materials Program of the Division of Research, U. S. Atomic Energy Commission.

†Present address: Wright State University, Dayton, Ohio 45431.

‡Parts of this work are included in the M. S. Thesis of D. F. Johnson. Present address: U. S. Air Force Academy, Colorado 80840.

[1]H. M. Simpson and A. Sosin, preceding paper, Phys. Rev. B 5, 1382 (1972)(hereafter referred to as paper 1).

[2]J. S. Koehler, *Imperfections in Nearly Perfect Crystals* (Wiley, New York, 1952).

[3]A. Granato and K. Lücke, J. Appl. Phys. 27, 583 (1956).

[4]J. A. DiCarlo, C. L. Snead, Jr., and A. N. Goland, Phys. Rev. 178, 1059 (1969); see, also, A. Sosin, Acta Met. 10, 390 (1962).

[5]A. Sosin, L. L. Bienvenue, and H. Schlein, Rev. Sci. Instr. 29, 657 (1958).

[6]A. Sosin and D. W. Keefer, *Advances in Materials Research* (Wiley, New York, 1968), Vol. 2.

[7]H. M. Simpson, A. Sosin, G. R. Edwards, and S. L. Seiffert, Phys. Rev. Letters 26, 897 (1971).

[8]H. M. Simpson, A. Sosin, and S. L. Seiffert, J. Appl. Phys. 42, 3977 (1971).

[9]R. L. Nielsen, Ph. D. thesis (University of Pittsburgh, Pennsylvania, 1968) (unpublished).

[10]H. S. Carslaw and J. C. Jaeger, *Operational Methods in Applied Mathematics* (Dover, New York, 1963), p. 119.

[11]A. C. Damask and G. J. Dienes, *Point Defects in Metals* (Gordon and Breach, New York, 1963), pp. 79 and 80.